Multiple CMT source analysis of the 2004 Sumatra earthquake

Victor C. Tsai, Meredith Nettles, Göran Ekström, and Adam M. Dziewonski
Department of Earth and Planetary Sciences, Harvard University, Cambridge, Massachusetts, USA

Received 14 June 2005; revised 27 July 2005; accepted 10 August 2005; published 9 September 2005.

[1] While it is agreed that the great Sumatra earthquake of December 26, 2004 was among the largest earthquakes of the past century, there has been disagreement on how large it was, which part of the fault ruptured, and how the rupture took place. We present a centroid-moment-tensor (CMT) analysis of the earthquake in which multiple point sources are used in the inversion to mimic a propagating slip pulse. The final model consists of five point sources, with the southernmost sources accounting for the majority of the moment release. The presumed fault planes of the southern sources strike northwest, while those in the north strike northeast, consistent with the geometry of the subduction trench. Slip on the fault is found to be more oblique in the north than in the south. The inversion with five sources leads to a moment magnitude for the Sumatra earthquake of M_W = 9.3, consistent with estimates from long-period normal-mode amplitudes. **Citation:** Tsai, V. C., M. Nettles, G. Ekström, and A. M. Dziewonski (2005), Multiple CMT source analysis of the 2004 Sumatra earthquake, *Geophys. Res. Lett.*, *32*, L17304, doi:10.1029/2005GL023813.

1. Introduction

[2] The great Sumatra earthquake of December 26, 2004 was one of the largest earthquakes of the past century. Standard Harvard centroid-moment-tensor (CMT) analysis [*Dziewonski et al.*, 1981; *Ekström et al.*, 2005] of this event provided a point-source mechanism and moment magnitude (M_W) of 9.0. *Ammon et al.* [2005] have produced 3 different model slip distributions, each of which has $9.0 < M_W < 9.2$. *Park et al.* [2005] find that a model with $M_0 = 6.5 \times 10^{29}$ dyne-cm (M_W = 9.1) explains normal-mode spectral data. Work by *Stein and Okal* [2005] analyzing long-period normal modes ($_0S_2$, $_0S_3$ and $_0S_4$) suggests a larger seismic scalar moment of $M_0 = 1.0 \times 10^{30}$ dyne-cm, equivalent to M_W = 9.3. These authors argue that the most likely source of the additional moment release they detect is slow slip in the northern aftershock zone of the Sumatra earthquake. *Banerjee et al.* [2005] estimate a moment magnitude of 9.1–9.2 based on geodetic data and argue for even slower moment release. Other geodetic analyses [*Vigny et al.*, 2005] suggest that no slow slip is required.

[3] The original CMT analysis was limited by its simple parameterization of the earthquake as a point source in space with a prescribed, triangular moment-rate function. The large centroid time shift of 139 s found in the standard CMT analysis and the results of later studies [e.g., *Ammon et al.*, 2005] suggest that the earthquake had a total duration of 300–600 s. Because the original CMT analysis was conducted in the 300–500 s pass band, it is likely that the result of that analysis does not provide an accurate representation of the overall rupture characteristics. To allow for the representation of greater complexity during the rupture process, and to account for moment release occurring over the full duration of the earthquake, we model the Sumatra earthquake with a series of point sources distributed in space and time.

0094-8276/05/2005GL023813$05.00

2. Analysis

[4] We present a modified CMT analysis in which we fit a model with five sources to mantle-wave data filtered in the 200–500-s period range. The data we use were recorded by the IRIS Global Seismographic Network (GSN) and represent a similar dataset to that used in the original Harvard CMT. We edit seismograms recorded during approximately the first nine hours after the earthquake to select only high quality, on-scale segments of the records. A total of 81 stations and 217 components are included in the final analysis.

[5] In the multiple-source CMT analysis, we determine moment-tensor elements and centroid parameters for a set of several sources simultaneously. As in the standard, single-source CMT analysis, allowing for perturbations to the centroid location and time introduces a nonlinearity in the problem, and the best-fit solution is therefore obtained by iterative inversion. A starting centroid location and time must be provided for each source. Here, we also use an iterative approach to the inclusion of successive sources. We first invert for the centroid parameters for a single source. A second source is then introduced with an initial location approximately 1°N of the single-source location, with a time delay of approximately 30 s. This time delay is chosen with a rupture speed of ~3 km/s in mind [*Ammon et al.*, 2005; *Ishii et al.*, 2005]. The locations and times of both sources are then allowed to move to fit the data. The times and locations of the two sources are unaffected by the initial choice of the location and time for the second source. All starting locations between 1° to 3°N, −2° to 2°E and with a time delay of 20–80 s relative to the first source lead to the same final locations and times for these sources. The inversion with three sources builds upon the previous inversion in the same way the two-source inversion builds upon the one-source result. The same best-fit result is attained for a wide range of initial values.

[6] Inversions with four and five sources are conducted in a similar fashion. The results in these cases depend more strongly on the initial values for the locations and times. The variance reduction can always be improved by including more sources, and we therefore test the statistical significance of the improvement in variance reduction achieved by including these sources. We compare models in which sources four and five lie along the fault with

Table 1. Inversion Results for Source Models With Varying Numbers of Sources[a]

# of Sources	Residual Variance	Lat N (deg)	Long E (deg)	Time (sec)	Moment	Total Moment	Total M_W
1	0.25002	3.22	94.33	127.1	0.422	0.422	9.02
2	0.20190	3.07	94.45	110.2	0.432	0.554	9.10
		4.20	93.13	196.2	0.122		
3	0.13376	3.10	94.62	94.4	0.320	0.769	9.19
		5.02	93.14	170.3	0.298		
		7.78	91.73	299.7	0.151		
4	0.12325	3.15	94.64	93.0	0.298	0.875	9.23
		5.22	93.04	162.5	0.329		
		8.30	91.45	285.9	0.206		
		11.09	90.21	392.5	0.042		
5	0.11110	3.27	94.60	93.0	0.318	1.166	9.31
		5.39	93.16	162.6	0.387		
		8.39	91.91	281.2	0.275		
		11.19	91.30	378.5	0.105		
		13.29	92.14	490.4	0.081		

[a]Times are relative to 00:58:53.5 UT December 26, 2004. The depths of all sources are constrained at 25 km as discussed in the text. Moment is in units of 10^{30} dyne-cm.

models in which those sources are placed in random locations. We perform a hypothesis test with the null hypothesis being no difference in residual variance between the random and non-random cases. Using the distribution of residual variance at various depths along the fault as the sample distribution, we reject the null hypothesis at the 99.9% confidence level. The reduction in residual variance that results from including additional sources is thus not due only to an increase in the number of free parameters. An inversion with six sources results in only a marginal improvement in fit over the five-source model and we therefore choose to limit our analysis to five sources.

[7] The long-period waveforms provide limited constraints on centroid depth, and we therefore fix all centroid depths at 25 km. The main effect of changing the source depths is to produce a change in the dip angles of the sources, which leads to a change in the scalar moment. In general, larger estimates of dip lead to smaller estimates of scalar moment. Fixing the source depths at 20 km or 30 km results in slightly steeper dip angles and total scalar moments that are smaller than that of our preferred solution by 11% and 19%, respectively; the misfit to the data also increases. Other source depths lead to shallower or steeper dips, with larger or smaller scalar moments, but no inversion fixed at depths between 14 km and 30 km leads to dips as steep as those estimated from slab contours (12°–18°) [*Ammon et al.*, 2005]. The timing, focal geometries, and relative sizes of the sources do not change significantly as a result of changes to the source depth.

3. Results

[8] As detailed in Table 1, the inversion for a single source results in a moment of 4.22×10^{29} dyne-cm, similar to that from the standard CMT. The addition of the second source lowers the residual variance by a substantial amount (19%) and increases the total moment by 31%. The moment of the first source increases slightly (2%) with the inclusion of the second source. The inclusion of the third source reduces the residual variance by 34% relative to the two-source model, though the moment of this source is only 36% of that of the original, single-point-source moment. In this step, the total moment becomes more evenly distributed between the individual sources, with the moment of the second source more than doubling in size. We interpret these results as implying a distribution of three areas of large moment release.

[9] The inclusion of sources four and five has a less dramatic effect on the residual variance, but including each source leads to a statistically significant improvement in fit. We note that the addition of each source increases the total moment of the earthquake by an amount greater than its individual contribution to the moment. For example,

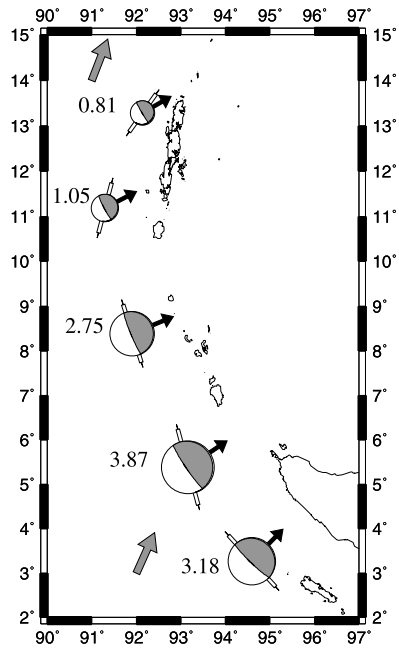

Figure 1. Locations and focal mechanisms of the five CMTs of our final model. The areas of the focal mechanisms are proportional to their scalar moments, which are given next to each mechanism in units of 10^{29} dyne-cm. The needles denote the strike directions of the shallowly dipping nodal planes; the black arrows denote the slip directions projected onto the horizontal plane. The gray arrows show the long-term plate motions of the Indian plate relative to the Eurasian plate [*DeMets et al.*, 1994].

Table 2. Source Parameters for the Final, Five-Source Model[a]

Source	Strike	Dip	Rake	Moment	M_W	ε
I	318	6.4	94	0.318	8.94	0.00
II	345	6.3	109	0.387	9.00	0.00
III	343	5.8	95	0.275	8.90	0.02
IV	15	8.4	132	0.105	8.62	0.04
V	35	8.1	155	0.081	8.54	0.01
Comp	343	6.1	107	1.15	9.31	0.02

[a]Strike, dip and rake are given in degrees. Moment is given in units of 10^{30} dyne-cm. ε describes the relative size of the non-double-couple component of the moment tensor and is calculated as $-e_2/\max(|e_1|,|e_3|)$ where e_i are the ordered eigenvectors of the moment tensor. Values for a composite ("Comp") solution obtained by summing the moment-tensor components of the individual sources are also listed. The centroid location and time for the composite source are 6.6°N, 93.0°E and 214 s.

although source five has a moment of only 0.08×10^{30} dyne-cm, including this source increases the total moment by 0.29×10^{30} dyne-cm relative to the four-source inversion.

[10] The final five-source model is depicted in Figure 1 and source parameters are listed in Table 2. The total moment obtained is 1.17×10^{30} dyne-cm, equivalent to moment magnitude $M_W = 9.3$. We find two large slip patches (27% and 33% of the total moment) in the southern portion of the fault, the locations of which roughly agree with the locations of regions of high slip in the *Ammon et al.* [2005] models. However, the moment release in these two areas is substantially larger than suggested by the results of *Ammon et al.* [2005]. This is particularly true for the northern of the two sources. Another large slip patch (24% of the total moment) is located farther north (8.4°N). The moment release at 11°N represents about 9% of the total, with the final 7% at 13°N.

[11] A composite moment-rate function is shown in Figure 2. A large fraction of the total moment is released in the first 200 seconds of the rupture, but substantial moment is released later as well, peaking with source three just prior to 300 seconds and continuing until more than 500 seconds after the initiation of rupture. Of the three *Ammon et al.* [2005] models, our results have the best agreement with model III in both the slip distribution and moment-rate function, though our results imply a larger moment release at all points along the fault than any of their models. The locations of our southern three sources also agree well with the locations of highest radiated energy in the model of *Ishii et al.* [2005] and the locations of the northern two sources agree with the northern extent of that model.

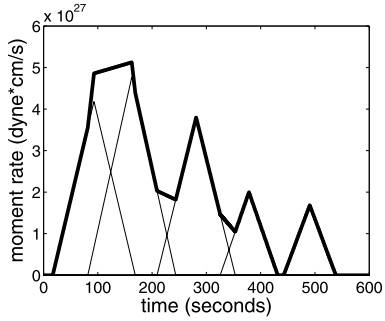

Figure 2. Source time function. The thin black lines denote the individual sources. The heavy black line denotes the sum. Source durations were chosen to satisfy $t = 2.2 \times 10^{-8} \times (M_0)^{1/3}$ [*Ekström and Engdahl*, 1989; *Ekström et al.*, 2005], where t = time (s) and M_0 = moment (dyne-cm). The source durations are fixed parameters in the inversion. The zero time corresponds to the hypocentral time of 00:58:53.5.

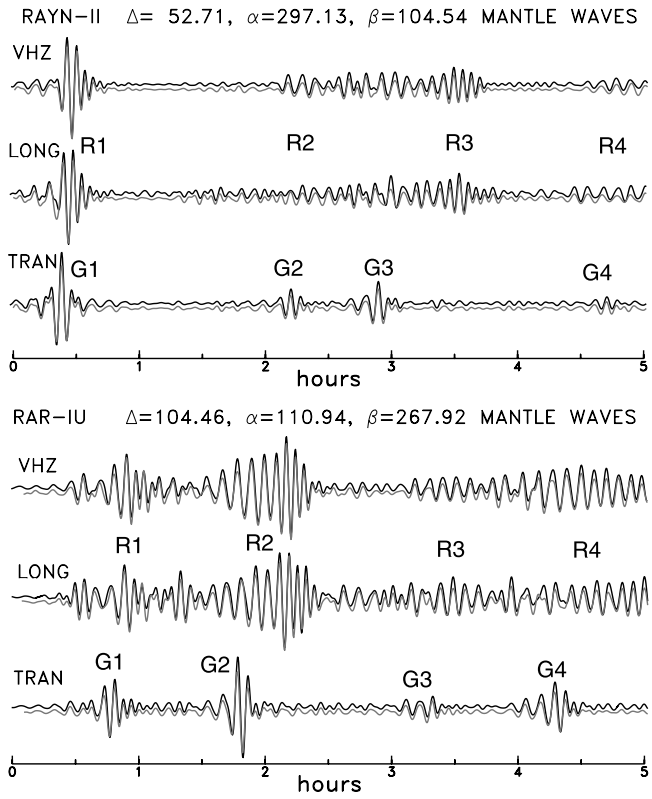

Figure 3. Examples of fit to seismograms achieved using the source model determined in this study. Black lines show data seismograms; gray lines show synthetic seismograms for the five-source model, offset slightly for clarity. Station RAYN lies roughly in the direction of rupture propagation. The odd arrivals (minor arc and subsequent orbits) are enhanced in amplitude. Station RAR lies roughly in the direction opposite to rupture propagation. The even arrivals (major arc and subsequent orbits) are enhanced in amplitude. Δ is the distance (in °) of the station from the earthquake. α is the azimuth of the station relative to the earthquake. β is the azimuth of the earthquake relative to the station. VHZ = vertical; LONG = longitudinal; TRAN = transverse. The zero time is as in Table 1.

[12] The effects of directivity are clear in the data we analyze. As shown in Figure 3, the amplitudes of the minor-arc arrivals are enhanced in the azimuth of rupture propagation while the amplitudes of the major-arc arrivals are enhanced in the opposite azimuth. The use of multiple sources allows us to model these directivity effects well. From the centroid locations and times of the sources, we calculate a 'propagation velocity,' by which we mean the distance between successive centroid locations divided by the time between them. Some care must be taken in interpreting this velocity, as it represents the propagation of moment release only in some averaged sense. The

velocities between adjacent sources (I–II, etc.) are respectively 4.1, 3.0, 3.3, and 2.2 km/s. The rupture thus appears to have begun fast and slowed after passing source II, slowing again after passing source IV, in agreement with the geodetic estimates of *Vigny et al.* [2005].

[13] The total moment (1.17×10^{30} dyne-cm) we obtain agrees well with the estimate (1.0×10^{30} dyne-cm) of *Stein and Okal* [2005], but our result does not require a component of moment release that is sufficiently slow to excite only the longest-period normal modes. We interpret our results as indicating that most of the moment was released in the early, southern portion of the faulting, and that the earthquake rupture progressed northward at typical rates. The final 16% of the moment corresponding to the northern portion of the fault also appears to have been released at a normal rate.

[14] The focal mechanisms of the five sources change systematically from south to north. The strike of the mechanisms rotates clockwise (see Table 2), in good agreement with the geologically observed change in strike of the subduction interface. The slip vectors rotate from nearly pure thrust to oblique slip with a large strike-slip component, again consistent with the geometry of the subduction interface and, in general, with plate motions. However, slip directions differ markedly from the direction of long-term plate motion between India and Eurasia [*DeMets et al.*, 1994], a result consistent with significant extensional and strike-slip deformation in the overriding plate. Many upper-plate aftershocks have strike-slip focal mechanisms, especially in the region near 8°N, where the discrepancy between slip direction and long-term plate motions is largest and where we find high moment release in our model. The aftershocks in this region include the Nicobar swarm of late January 2005 [*Nettles et al.*, 2005], which were primarily strike-slip and normal events in the upper plate. Our model suggests that near 8° N the Sumatra earthquake may have released a substantial portion of the stress normal to the interface but left a significant amount of stress in the fault-parallel direction, which is in the process of being accommodated as strike-slip earthquakes in the adjacent region.

[15] Finally, it should be noted that our analysis cannot distinguish between a model with a few, discrete locations of large slip and a model with more uniform slip. However, our results are indicative of at least three, and possibly five, regions of concentrated moment release. This view is consistent with the non-uniform slip distributions obtained by *Ammon et al.* [2005] and *Ishii et al.* [2005].

[16] **Acknowledgments.** We thank H. Kanamori, C. Ammon, M. Antolik, R. Bürgmann, M. Ishii, T. Lay and two anonymous reviewers for helpful comments. The GSN data analyzed were collected and distributed by the Incorporated Research Institutions for Seismology (IRIS) and the USGS. This research was supported by a Harvard University James Mills Peirce Fellowship and a National Science Foundation (NSF) Graduate Research Fellowship (VCT) and by NSF grant EAR-0207608.

References

Ammon, C. J., et al. (2005), Rupture process of the 2004 Sumatra-Andaman earthquake, *Science*, *308*, 1133–1139.

Banerjee, P., F. F. Pollitz, and R. Bürgmann (2005), The size and duration of the Sumatra-Andaman earthquake from far-field static offsets, *Science*, *308*, 1769–1772.

DeMets, C., R. G. Gordon, D. F. Argus, and S. Stein (1994), Effect of recent revisions to the geomagnetic reversal time-scale on estimates of current plate motions, *Geophys. Res. Lett.*, *21*, 2191–2194.

Dziewonski, A. M., T. A. Chou, and J. H. Woodhouse (1981), Determination of earthquake source parameters from waveform data for studies of global and regional seismicity, *J. Geophys. Res.*, *86*, 2825–2852.

Ekström, G., and E. R. Engdahl (1989), Earthquake source parameters and stress distribution in the Adak Island region of the central Aleutian Islands, Alaska, *J. Geophys. Res.*, *94*, 15,499–15,519.

Ekström, G., A. M. Dziewonski, N. N. Maternovskaya, and M. Nettles (2005), Global seismicity of 2003: Centroid-moment-tensor solutions for 1087 earthquakes, *Phys. Earth Planet. Inter.*, *148*, 327–351.

Ishii, M., P. M. Shearer, H. Houston, and J. E. Vidale (2005), Rupture extent, duration, and speed of the 2004 Sumatra-Andaman earthquake imaged by the Hi-Net array, *Nature*, *435*, 933–936.

Nettles, M., G. Ekström, A. M. Dziewonski, N. N. Maternovskaya, and V. C. Tsai (2005), Source characteristics of the great Sumatra earthquake and its aftershocks, *Eos Trans. AGU*, *86*, Jt. Assem. Suppl., Abstract U43A-01.

Park, J., et al. (2005), Earth's free oscillations excited by the 26 December 2004 Sumatra-Andaman earthquake, *Science*, *308*, 1139–1144.

Stein, S., and E. A. Okal (2005), Speed and size of the Sumatra earthquake, *Nature*, *434*, 581–582.

Vigny, C., et al. (2005), Insight into the 2004 Sumatra-Andaman earthquake from GPS measurements in southeast Asia, *Nature*, *436*, 201–206.

A. M. Dziewonski, G. Ekström, M. Nettles, and V. C. Tsai, Department of Earth and Planetary Sciences, Harvard University, Cambridge, MA 02138, USA. (vtsai@fas.harvard.edu)